Optical scatter imaging: subcellular morphometry *in situ* with Fourier filtering

Nada N. Boustany, Scot C. Kuo, and Nitish V. Thakor

Department of Biomedical Engineering, Johns Hopkins University, Baltimore, Maryland 21205

Received February 2, 2001

We demonstrate a quantitative optical scatter imaging (OSI) technique, based on Fourier filtering, for detecting alterations in the size of particles with wavelength-scale dimensions. We generate our scatter image by taking the ratio of images collected at high and low numerical aperture in central dark-field microscopy. Such an image spatially encodes the ratio of wide to narrow angle scatter and hence provides a measure of local particle size. We validated OSI on sphere suspensions and live cells. In live cells, OSI revealed biochemically induced morphological changes that were not apparent in unprocessed differential interference contrast images. Unlike high-resolution imaging methods, OSI can provide size information for particles smaller than the camera's spatial resolution. © 2001 Optical Society of America

OCIS codes: 110.0180, 170.1530, 170.3880, 070.6110, 290.5850.

Light-scattering spectroscopy has been used to observe dynamic alterations in cellular and subcellular morphology. In particular, angular scatter data have been extensively employed in cell analysis, such as flow cytometry, to probe intracellular morphology and infer morphological information about objects that cannot be optically resolved. Scatter intensities at multiple angles can be collected with a goniometer and a single photodetector[1–3] or by many detectors positioned at different angles around the specimen.[4] Alternatively, the sample's diffraction pattern can be analyzed by use of Fourier optics to infer angular scatter.[5–8] Those previous studies provide extensive spectroscopic angular-scatter data. However, to identify the scattering sources contributing to the signal, one must image the sample under study separately to infer the location of the incident beam or to direct this beam toward a specific microscopic region of the sample. In this Letter we propose to incorporate angular-scatter information directly into a specimen's image. We demonstrate a method of combining light-scattering spectroscopy with imaging microscopy to produce images that directly encode a morphometric parameter within the full field of view. This optical scatter imaging (OSI) technique is validated on polystyrene sphere standards, and its applicability to live cell analysis is further demonstrated in a biological process that is known to involve changes in organelle morphology. As we will show, an important attribute of OSI is that it provides sensitivity to particles near the resolution limit of the microscope even with a camera pixel size that cannot resolve these particles.

OSI employs dark-ground (or dark-field) microscopy, in which transmitted light is optically blocked out, yielding images whose intensity is directly proportional to the intensity of the light scattered by the particles within a given specimen. For spheres, Mie theory[9] gives the dependence of scatter intensity on particle size x, $x = \pi D/\lambda$ (λ, wavelength; D, sphere diameter), and index ratio m, $m = n_p/n_m$ (n_p, particle refractive index; n_m, surrounding medium index). Briefly, the larger the particle, and the larger its refractive-index ratio, m, the larger its scattering cross section, and the brighter it will appear in central dark-field imaging. Moreover, the ratio of wide- to narrow-angle scatter generally decreases with increasing diameter. In this first investigation of OSI, we use this ratio as an indicator of particle size. In a transmission microscope utilizing the central dark-ground method, wide and narrow angles of scatter will be selected by variation of the diameter of the aperture in a Fourier plane conjugate to the objective's back focal plane. In general, our method consists of directly mapping selective scatter information into the imaging plane. Although we have chosen to look first at the ratio of wide-to-narrow-angle scatter, other Fourier plane apertures could be designed to select different scattering parameters.

In our optical setup (Fig. 1), the specimens were mounted on the stage of an inverted microscope. We adjusted the microscope condenser to central Köhler illumination, with a condenser numerical aperture (NA) of 0.03 (condenser front aperture closed). For illumination, light from the microscope's halogen lamp was filtered to yield an incident red beam, $\lambda = 630 \pm 5$ nm. The images were collected with a 60× oil-immersion

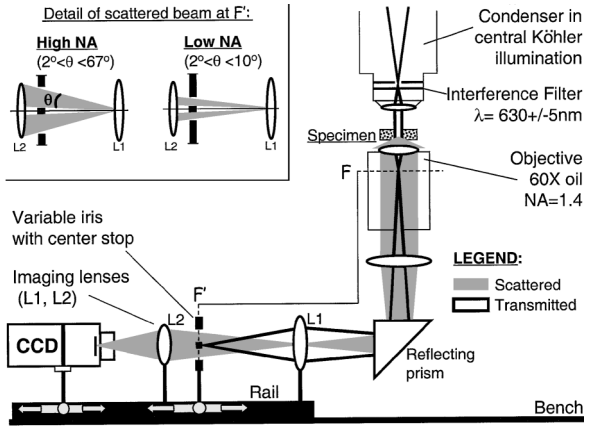

Fig. 1. OSI setup. F, objective's back focal plane; F and F′ are conjugate Fourier planes. The scattered light (gray beam) is used to image the specimen on the CCD, and the transmitted light (black ray traces) is blocked at F′. The inset shows the scattered angles passed at the high- and low-NA settings.

0146-9592/01/141063-03$15.00/0

objective, NA = 1.4. In a plane conjugate to the back focal plane of the objective, we placed a beam stop in the center of an iris with variable diameter. The variable iris collected light scattered within a solid angle, θ, bound by $2° < \theta < 10°$ for low NA and $2° < \theta < 67°$ for high NA. The diameter of the beam block (0.5 mm), the smallest iris diameter, and the NA of the microscope objective defined the angles 2°, 10°, and 67°, respectively. For each specimen studied, two sequential images were acquired at high and low NA by manual adjustment of the diameter of the iris. OSI images were binned into pixels, which corresponded to regions in the object between 2 μm × 2 μm and 2.5 μm × 2.5 μm, depending on the final magnification. For each specimen we measured the optical scatter image ratio (OSIR) at each pixel bin by dividing the high-NA image by the low-NA image. A background signal was subtracted from each image.[10] Given the aperture settings used, the OSIR can be defined as

$$\mathrm{OSIR} = \frac{\int_{\phi=0}^{360^\circ}\int_{\theta=2^\circ}^{67^\circ} F(\theta,\phi)\sin\theta\,\mathrm{d}\theta\,\mathrm{d}\phi}{\int_{\phi=0}^{360^\circ}\int_{\theta=2^\circ}^{10^\circ} F(\theta,\phi)\sin\theta\,\mathrm{d}\theta\,\mathrm{d}\phi}, \qquad (1)$$

where $F(\theta, \phi)$ gives the intensity of the light scattered in a given direction defined by the angles θ and ϕ. θ is the angle between the scatter direction and the direction of propagation of the incident light, and ϕ is the azimuthal angle of scatter. For spheres, the value of F is computed by numerical solution of Mie theory.[9] For particles of arbitrary shape, other numerical methods such as the finite-difference time-domain technique can be used.[1,11]

To illustrate the dependence of OSIR on particle size, we used well-mixed aqueous suspensions of polystyrene spheres with diameters D spanning 0.3–6 μm. The samples were 75 μm thick and had a scattering coefficient, μ_S in the range 0.005–0.025 $\mu\mathrm{m}^{-1}$. The index ratio is $m = n_{\mathrm{polystyrene}}/n_{\mathrm{water}} = 1.6/1.33 = 1.2$. Figure 2 shows the mean pixel value and the standard deviation in the center region of each OSI image plotted versus sphere diameter (open circles). These center regions (25 × 25 pixels) are displayed on the left-hand side of the figure. The solid curve represents OSIR predictions as calculated from Mie theory for $m = 1.2$ and shows excellent agreement with experiment. For comparison, the dashed curve shows the theoretical prediction for $m = 1.06$. For $m \sim 1$, the curve remains flat after 2-μm diameter and does not exhibit the sharp oscillation at $D \sim 3$ μm. For $0.2 < D < 1.5$ μm, the scatter ratio decreases monotonically with diameter and is independent of refractive index in the range $1 < m < 1.2$. The diameter range, $0.2 < D < 1.5$ μm, corresponds to $1.3 < x < 10$, $x = \pi D/\lambda$. Varying λ may be utilized to shift this D range.

Having established the size sensitivity of OSI by using spheres, we applied the method to cells, which naturally contain scatterers of various sizes, such as the nucleus (4–15 μm) and the mitochondria (0.5–2 μm). Particle-size variation should therefore be seen across the cell. The top panels of Fig. 3A show differential interference contrast (DIC) and OSI images of a normal endothelial cell. The nucleus region (N)/(C) and the cytoplasm containing the mitochondria are clearly differentiated in the OSI image, despite a much larger pixel size than the accompanying DIC image. In the OSI image, owing to the nonlinear inverse relationship between OSIR and particle diameter, regions with small particles (C) appear brighter than regions with large particles (N). For normal organelles, the refractive-index ratio is $m \sim 1$. Thus, taking the sphere data (Fig. 2, $m = 1.06$) as a first-order approximation of organelle scattering, we find that $2 \le \mathrm{OSIR} \le 3$ corresponds to $1\ \mu\mathrm{m} \le D \le 2\ \mu\mathrm{m}$ in the cytoplasm. This diameter range is consistent with average mitochondrial size in endothelial cells and corroborates previous results

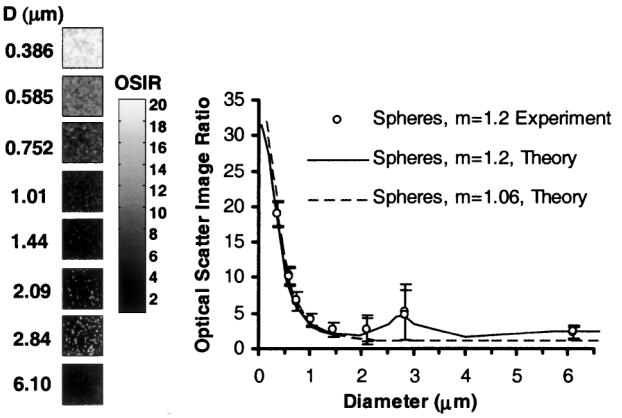

Fig. 2. OSI images and measurement of the OSIR in aqueous suspensions of polystyrene spheres. Experimental data (open circles, refractive-index ratio $m = 1.2$), theoretical predictions (solid curve, $m = 1.2$; dashed curve, $m = 1.06$). The data in the graph are the mean plus or minus the standard deviation of pixel values in the images shown on the left.

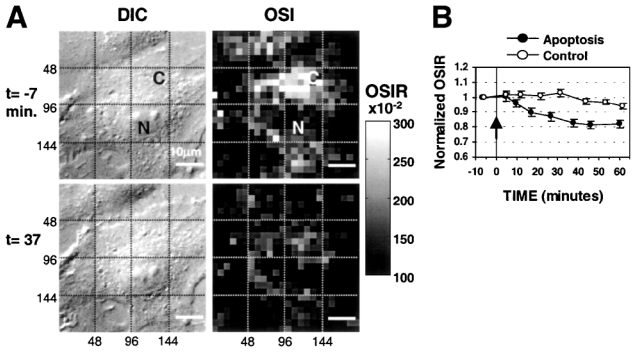

Fig. 3. A, DIC and OSI images of a representative cell undergoing apoptosis. Top panels, normal cell; bottom panels, the cell 37 min after apoptosis induction. C, cytoplasm; N, nucleus. B, Time course of the OSIR in the cytoplasm of cells undergoing apoptosis (filled circles) compared with control cells kept in the normal growth medium (open circles). Apoptosis was induced at $t = 0$ (arrow). The error bars represent the 95% confidence interval of the mean. The OSIR was normalized to values at $t = -7$ min.

showing that mitochondria are a major contributor to tissue light scattering.[12]

To illustrate the biological relevance of OSI, we investigated the possibility of detecting subcellular morphological changes in cells undergoing apoptosis, or programmed cell death. Apoptosis is a fundamental biological process involving alterations in mitochondrial volume.[13,14] We induced endothelial cells to undergo apoptosis by adding staurosporine to the growth medium. The apoptotic cells were compared with control cells kept in the normal growth medium. Figure 3A depicts OSI and DIC images of a representative cell before (top panels) and after (bottom panels) apoptosis induction. After the onset of apoptosis ($t = 37$ min), the OSI image shows a decreased OSIR within the cytoplasm and no change in the nucleus. Moreover, the OSIR decrease in the cytoplasm was not accompanied by any significant change in the DIC images. The OSIR decrease was reproducible. Averaged over the whole cell population (Fig. 3B), the OSIR decreased significantly in the apoptotic cells (filled circles, $n = 58$) but did not vary in the control cells (open circles, $n = 55$). Since the OSIR is independent of m at $D \sim 1.5$ μm, a change in refractive index cannot fully account for the decrease in OSIR. Thus, based on Fig. 2, the decrease in OSIR corresponds to an increase in the average particle size within the cytoplasm and is consistent with reported mitochondrial swelling.[14] Nonetheless, further biochemical analysis and scatter predictions for nonspherical objects are necessary to validate fully the underlying biological process. At present our data show that OSI can reveal biochemically induced intracellular dynamics, which might remain undetected in unprocessed microscopic images.

OSI resolution is determined by the diffraction limit as in conventional microscopy. Owing to the objective's finite aperture, OSI could not be utilized to discriminate particles that are small enough to have little variation in scattering intensity in the range 0°–67° (high-NA angle). For spheres with $m = 1.2$, this theoretical limit corresponds to particles with $x \leq 0.6$ ($x = \pi D/\lambda$), as calculated from Mie theory. As such, OSI resolution is defined by the finite limit of the OSIR as scatterer size goes to 0. This resolution limit is determined at the Fourier plane rather than the image plane. The power of the technique lies in the Fourier optical filtering, which allows for resolution of particle size below the camera's pixel resolution.

In fact, if the pixel size is less than the size of a particle, the OSIR will give a local wide-to-narrow-angle scatter ratio, which may not correspond to the scatter ratio expected from theory. For example, the OSIR calculated in a pixel bin located at the edge of a sphere will not necessarily result in the ratio predicted from Mie theory, which applies to the whole sphere. Decisions about pixel binning can be made after OSIR calculation. Because the low-NA image intensity is approximately constant over a given object, the average value of the OSIR in the pixel bin will be similar whether the pixels are binned before or after the OSIR is computed.

Since OSI is effectively an analog Fourier filtering technique, in which the ratio of two spatially filtered signals is calculated on a pixel-by-pixel basis, similar data could be obtained digitally by Fourier filtering DIC or other high-resolution images. In contrast to analog OSI, digital OSI is limited by the spatial frequency content of the image, which must match that set by the diffraction limit of the optics. In particular, the magnification must correspond to less than $\lambda/2(\mathrm{NA})$ per pixel, as confirmed with polystyrene sphere suspensions (not shown). However, an adequate diffraction-limited image may not always be available. On the other hand, analog OSI remains applicable to low-resolution imaging devices and at low and intermediate magnification, at which a wider field can be viewed. In the case of analog OSI, theoretical simulations from spheres showed that a NA as low as 0.5 still results in good OSIR sensitivity in the range $1.3 < x < 10$, such that lower-magnification objectives could be used.

In summary, we have demonstrated a simple and effective method of detecting subtle morphological changes, *in situ*, in particles with wavelength-scale dimensions. We believe that OSI may have significant applications in cell biology and biotechnology, where it can be applied to live cell morphometry without the need to resolve individual organelles or to use fluorescent dyes.

N. N. Boustany was supported by a fellowship from the Whitaker Foundation. We thank Doug Murphy and George Oyler for fruitful discussions. N. N. Boustany's e-mail address is nnboustany@alum.mit.edu.

References

1. R. Drezek, A. Dunn, and R. Richards-Kortum, Appl. Opt. **38,** 3651 (1999).
2. J. R. Mourant, J. P. Freyer, A. H. Hielscher, A. A. Eick, D. Shen, and T. M. Johnson, Appl. Opt. **37,** 3586 (1998).
3. L. J. Johnson, D. F. Hanley, and N. V. Thakor, J. Neurosci. Methods **98,** 21 (2000).
4. P. J. Wyatt, Anal. Chim. Acta **272,** 1 (1993).
5. Z. Schiffer, Y. Ashkenazy, R. Tirosh, and M. Deutsch, Appl. Opt. **38,** 3626 (1999).
6. D. E. Burger, J. H. Jett, and P. F. Mullaney, Cytometry **2,** 327 (1982).
7. B. Turke, G. Seger, M. Achatz, and W. Seelen, Appl. Opt. **17,** 2754 (1978).
8. P. D. Kaplan, V. Trappe, and D. A. Weitz, Appl. Opt. **38,** 4151 (1999).
9. H. C. van de Hulst, *Light Scattering by Small Particles* (Dover, New York, 1981), Chap. 9.
10. A solvent sample consisting of the medium in which the sample was prepared served to provide the background scatter signal owing to the microscope optics.
11. A. Dunn, C. Smithpeter, A. J. Welch, and R. Richards-Kortum, J. Biomed. Opt. **2,** 262 (1997).
12. B. Beauvoit, S. M. Evans, T. W. Jenkins, E. E. Miller, and B. Chance, Anal. Biochem. **226,** 167 (1995).
13. For example, see L. J. Miller and J. Marx, Science **281,** 1301 (1998).
14. M. G. Vander-Heiden, N. S. Chandel, E. K. Williamson, P. T. Shumacker, and C. B. Thompson, Cell **91,** 627 (1997).